International Journal of Pharmaceutics 434 (2012) 444–452

Contents lists available at SciVerse ScienceDirect

International Journal of Pharmaceutics

journal homepage: www.elsevier.com/locate/ijpharm

Pharmaceutical Nanotechnology

Preparation of chains of magnetosomes, isolated from *Magnetospirillum magneticum* strain AMB-1 magnetotactic bacteria, yielding efficient treatment of tumors using magnetic hyperthermia

Edouard Alphandéry[a,b,*], François Guyot[a,c], Imène Chebbi[b]

[a] *Institut de minéralogie et de physique des milieux condensés, Université Pierre et Marie Curie, UMR CNRS 7590, 4 Place Jussieu, 75005 Paris, France*
[b] *Nanobacterie SARL, 36 boulevard Flandrin, 75016 Paris, France*
[c] *Université Paris Diderot, Sorbonne Paris Cité, Institut de Physique du Globe de Paris, 1 Rue Jussieu, 75005 Paris, France*

ARTICLE INFO

Article history:
Received 18 April 2012
Received in revised form 31 May 2012
Accepted 3 June 2012
Available online 12 June 2012

Keywords:
Magnetosomes
Magnetotactic bacteria
Cancer
Tumor
Chains of magnetosomes
Individual magnetomes
Alternating magnetic field
Magnetic hyperthermia

ABSTRACT

Chains of magnetosomes isolated from *Magnetospirillum magneticum* strain AMB-1 magnetotactic bacteria by sonication at 30 W during 2 h are tested for magnetic hyperthermia treatment of tumors. These chains are composed of magnetosomes, which are bound to each other by a filament made of proteins. When they are incubated in the presence of cancer cells and exposed to an alternating magnetic field of frequency 198 kHz and average magnetic field strength of 20 or 30 mT, they produce efficient inhibition of cancer cell proliferation. This behavior is explained by a high cellular internalization, a good stability in solution and a homogenous distribution of the magnetosome chains, which enables efficient heating. When the chains are heated during 5 h at 90 °C in the presence of 1% SDS, the filament binding the magnetosomes together is denatured and individual magnetosomes are obtained. By contrast to the chains of magnetosomes, the individual magnetosomes are prone to aggregation, are not stable in solution and do not produce efficient inhibition of cancer cell proliferation under application of an alternating magnetic field.

© 2012 Elsevier B.V. All rights reserved.

1. Introduction

Magnetic hyperthermia is a technique by which magnetic nanoparticles are either introduced or sent within tumors and heated under the application of an alternating magnetic field (AMF). The heat produced locally by the nanoparticles induces anti-tumoral activity. Magnetic hyperthermia has been used both on animal models and on humans to treat a series of different cancers, including breast cancer (DeNardo et al., 2007; Kikumori et al., 2009), prostate cancer (Johannsen et al., 2005, 2007; Kawai et al., 2005, 2008), glioblastoma (Maier-Hauff et al., 2011), and head and neck cancer (Zhao et al., 2012). Until now, most of the iron oxide nanoparticles tested were chemically synthesized with either a superparamagnetic or a weakly ferrimagnetic behavior at physiological temperature (Hergt et al., 2006, 2008; Hergt and Dutz, 2007; Bordelan et al., 2011). For an applied magnetic field of frequency and strength kept below a toxicity threshold of ~200 kHz and ~100 mT respectively (Ivkov et al., 2005), the specific absorption rate (SAR) of the chemically synthesized nanoparticles is lower by a factor of 2–100 than that of the biologically synthesized nanoparticles, called magnetosomes (Hergt et al., 2006, 2008; Hergt and Dutz, 2007). For this reason, there has been a surge of interest to carry out magnetic hyperthermia for cancer treatment using the magnetosomes (Hergt et al., 2005; Timko et al., 2009; Alphandéry et al., 2011a,b,c). In fact, the magnetosomes are monodomain, well-crystallized nanoparticles surrounded by a lipidic membrane with the unique property of being usually arranged in chains. They are synthesized by a group of bacteria, called magnetotactic bacteria, which use them as a compass to navigate in the direction of the earth magnetic field in search for optimal growth conditions. In a previous study (Alphandéry et al., 2011c), 1 mg of a suspension of chains of magnetosomes extracted from *Magnetospirillum magneticum* strain AMB-1 magnetotactic bacteria has been administered within breast tumors xeno-grafted under the skin of mice. After three applications of an alternating magnetic field during 20 min, tumors were totally eradicated in several mice. These results suggest that chains of magnetosomes extracted from AMB-1 magnetotactic bacteria are highly efficient for solid tumor treatment using magnetic hyperthermia (Alphandéry et al., 2011c).

In this article, we examine if the efficiency of chains of magnetosomes extracted from AMB-1 magnetotactic bacteria, designated

* Corresponding author at: Nanobacterie, 36 boulevard Flandrin, 75016 Paris, France. Tel.: +33 632697020.
E-mail address: edouardalphandery@hotmail.com (E. Alphandéry).

0378-5173/$ – see front matter © 2012 Elsevier B.V. All rights reserved.
http://dx.doi.org/10.1016/j.ijpharm.2012.06.015

as CM, is solely due to the high SAR of the magnetosomes or if it also arises from other factors such as a homogenous distribution of the magnetosome chains within the tissue or a faculty of the magnetosome chains to internalize within the cancer cells. To know the influence of the magnetosome chain arrangement on the efficiency of the therapy, we compare the properties of the chains of magnetosomes with those of individual magnetosomes, designated as IM, which are detached from the chains by heat and chemical treatments.

2. Materials and methods

2.1. Method used for the culture of the AMB-1 magnetotactic bacteria

Magnetotactic bacteria belonging to the species *M. magneticum*, strain AMB-1, available at the ATCC under the reference 700264, were cultivated in a volume of 1 l of bacterial growth medium. The cells were cultivated in microaerobic conditions, i.e. in a culture medium that has not been degassed, but is closed and not in contact with oxygen. The cells were inoculated in oxic conditions and the medium became more and more reduced while the cells grew and used oxygen. The culture of magnetotactic bacteria has been carried out in an incubator at 26 °C in a slightly modified MSGM liquid culture medium, whose composition is described below.

For a volume of 1 l, the standard culture medium contains 0.68 g of monobasic potassium phosphate, 0.85 g of sodium succinate, 0.57 g of sodium tartrate, 0.083 g of sodium acetate, 225 μl of 0.2% resazurine, 0.17 g of sodium nitrate, 0.04 g of L-ascorbic acid, 2 mL of a 10 mM solution of iron quinate, 10 mL of a solution of Wolfe's vitamins and 5 mL of a solution of Wolfe's minerals (Wolfe et al., 1987). The solution of iron quinate has been prepared by dissolving 0.19 g of quinic acid and 0.29 g of $FeCl_3 \cdot 6H_2O$ in 100 mL of distilled water. The pH of the culture medium was adjusted to 6.85 by using a 1 M solution of sodium hydroxide.

2.2. Preparation of the different suspensions containing the extracted chains of magnetosomes and individual magnetosomes

Two different types of magnetosomes have been isolated from AMB-1 magnetotactic bacteria, those arranged in chains and those forming individual nanoparticles. To prepare them, the cells were first harvested by centrifugation at 4 000 g during 20 min. The supernate was then removed and the cells were re-suspended in deionized water. To extract the chains of magnetosomes, 1 mL of cell suspension obtained as previously described was centrifuged again and re-suspended in a 10 mL Tris–HCl buffer of pH 7.4. The cellular suspension was then sonicated during 120 min at 30 W in order to lyse the cells and collect the CM. After sonication, the suspension containing the CM was separated from the cellular debris by positioning a strong neodynium magnet (0.1–1 T) next to the tube, and the magnetic material was then harvested. The supernate containing the cellular debris and other organic molecules was eliminated. CM were washed 10–20 times in deionized water at pH 7.4 and were then resuspended in deionized water. To prepare the suspensions containing the IM, the suspension containing the CM was heated during 5 h at 90 °C in the presence of 1% SDS. IM were separated from the biological material remaining after the treatment by using a strong neodynium magnet (0.1–1 T). The concentrations in maghemite of the various suspensions containing CM and IM were measured by absorption at 480 nm (Alphandéry et al., 2011c). The maghemite composition of the magnetosomes by measuring the saturation isothermal remanent magnetization of the extracted chains of magnetosomes and individual magnetosomes following the same method as that described previously (Alphandéry et al., 2008). The absence of the Verwey transition indicated that the magnetite had oxidized into maghemite. The CM and IM used for all experiments except the infra-red measurements were not lyophilized. In order to determine the functional groups at the surface of the CM and IM, infra-red absorption measurements have been carried out using a Nicolet FT-IR model 380 with resolution of 0.5 cm^{-1} and a number of scan of 30. For these measurements, suspensions of CM and IM with a concentration of 1 mg/mL in iron oxide were used.

2.3. Methods used for measuring the SAR and for heating the different suspensions of bacterial magnetosomes

The SAR of suspensions of CM and IM was measured for bacterial magnetosomes, which were either able or unable to rotate under the application of an AMF (Alphandéry et al., 2011a). The amount of heat produced in the gel by the CM and IM was low under the application of an AMF of frequency 108 kHz and magnetic field strength kept below 36 mT (Alphandéry et al., 2011a). To enhance the magnetosome heating efficiency during the in vitro and in vivo heating experiments, the frequency of the AMF was therefore increased up to 198 kHz and the average magnetic field strength was kept below 30 mT to avoid the formation of eddy currents, which can induce toxicity. The average magnetic field strength was estimated from the variation with time of the magnetic field strength. It was measured using a 2D magnetic field probe designed by the company Fluxtrol. The value of the average magnetic field strength measured experimentally with this probe was 1.8 times lower than the theoretical value of the magnetic field, estimated using the relation $B = \mu_0 NI/L$, where $\mu_0 = 4\pi \times 10^{-7}$ is the vacuum permeability, $N = 4$ is the number of spires in the coil, $I = 151$, 300, 419 or 600 A is the amplitude of the alternating current flowing through the spires and $L = 3.5$ cm is the length of the coil (Suppl. Table 1). The temperatures reached during the heating experiments were measured using a thermocouple microprobe (IT-18, Physitemp, Clifton, USA).

2.4. Percentage of inhibition and magnetization studies of HeLa and MDA-MB-231 cells incubated in the presence of the different suspensions of magnetosomes isolated from AMB-1 magnetotactic bacteria

The HeLa and MDA-MB-231 cells were purchased from the ATCC. The cell lines were cultivated in Dulbecco's model modified Eagle's medium supplement, which contained 10% fetal calf serum, 2 mM L-glutamine, 1 mM sodium pyruvate, and 50 U/mL streptomycin (all purchased from Life Technologies Inc.). Cell viability was evaluated using the so-called MTT (microculture tetrazolium) assay (Mosmann, 1938). This technique measures the ability of mitochondrial enzyme to reduce 3-(4,5-dimethylthiazol-2-yl)-2,5-diphenyltetrazolium bromide (purchased from Sigma, St Louis, MO, USA) to purple formazan crystals. MDA-MB-231 and HeLa cells were seeded at a density of 2.10^4 cells per well in 96-well flat-bottom plates (Falcon, Strasbourg, France) and incubated in completed culture medium for 24 h. Then, the culture medium was removed and replaced by 10% FCS-medium containing CM or IM with different concentrations in iron oxide (1 mg/mL, 500 μg/mL or 125 μg/mL). After 24 h of incubation, the cells were exposed (or not) to an AMF of frequency 198 kHz and average magnetic field strength of ~20 mT or ~30 mT during 20 min. After having been exposed to the AMF, the cells were incubated at 37 °C in a 5% CO_2 humidified atmosphere during 48 h. Following the incubation, cells were washed with phosphate buffered saline solution (PBS, Life Technologies) and incubated with 100 μl of MTT (2 mg/mL, Sigma–Aldrich) for an additional 4 h at 37 °C. The insoluble product was then dissolved by addition of 100 mL of DMSO (Sigma–Aldrich). The absorbance of the solubilized formazan pellet, which reflects

the relative viable cell number, was measured at 540 nm using a Labsystems Multiskan MS microplate reader. The measurements were carried out on DMSO solubilized formazan pellets using cells washed with PBS as a control (Yoshino et al., 2008). The experiments were carried out in triplicates.

2.5. Internalization and magnetization studies of MDA-MB-231 cells incubated in the presence of various suspensions of magnetosomes

5×10^5 MDA-MB-231 cells in suspension were mixed in 1 mL of a 10% FCS-medium containing suspensions of CM or IM with a fixed concentration in iron oxide of 1 mg/mL. The cells were exposed (or not) to an AMF of frequency 198 kHz and average field strength of ~20 mT during 5, 10, 15 and 20 min. Following the application of the AMF, the MDA-MB-231 cells were collected with a strong neodynium magnet (0.1–1 T). For each sample, 10^4 cells were used to quantify the mass of iron oxide per cell. Solutions containing various concentrations of $FeCl_3$ mixed with potassium thiocyanate (2 M) were prepared for calibration. Solutions containing one volume of HCl (6 N) mixed with 20 volumes of H_2O_2 were added to the cells to dissolve the iron oxide into Fe^{3+} ions and to denature all biological material. The cells were further lysed by sonication during 30 min at 30 W (0 °C) and mixed with a solution of potassium thiocyanate (2 M), which induces the formation of a complex composed of Fe^{3+} and SCN^-. Quantification of iron oxide was estimated by absorption measurements at 480 nm (UVICON 923, Bio-Tek, Kontron Instrument, Italy). The untreated MDAMB-231 cells were used as reference. The experiments were carried out in triplicates.

2.6. In vitro Prussian blue assay

MDA-MB-231 cells were seeded on Petri dishes (Ø 30 mm, density ~5×10^5 cells per Petri dish), grown during 24 h and incubated (or not) during 24 h in the presence of suspensions of CM or IM at a concentration of 142 μg/mL. Cells were washed two more time in PBS and fixed in 4% paraformaldehyde (PFA) (Sigma) during 15 min at 4 °C. MDA-MB-231 cells were washed twice more time in PBS and were then stained with Perl's Prussian blue solution during 20 min at 37 °C in an atmosphere containing 5% CO_2. Perl's Prussian blue solution was prepared by mixing two solutions of equal volumes containing 4% potassium ferrocyanide and 4% HCl. Staining (bright blue pigment: $Fe^{III}[Fe^{III}Fe^{II}(CN)_6]_3$) resulted from the reaction between Fe^{2+} or Fe^{3+} ions coming from the dissolved magnetosomes and the ferrocyanide ions. After having washed each Petri dish three times with PBS, Prussian blue staining was observed using an optical microscope. The experiments were carried out in triplicates.

2.7. Scanning electron microscopy, transmission electron microscopy and optical microscopy studies of MDA-MB-231 cells incubated in the presence of either chains of magnetosomes or individual magnetosomes

Scanning electron microscopy (SEM) studies were carried out using a FEG-SEM ultra 55 from Zeiss equipped with an energy dispersive X-ray analysis system (EDX). The samples studied by SEM contained MDA-MB-231 cancer cells incubated during 24 h in the presence of IM or CM. The cells were deposited on top of a carbon grid covered with a carbon film and fixed with NOVAprep, produced by Novacyt. Transmission electron microscopy (TEM) studies were also carried out using a JEOL 2100F-FEG operated at 200 kV. The samples studied by TEM contained 5 μl of suspensions of IM or CM deposited on top of a carbon grid. We waited for 2 h that the suspensions dried before carrying the experiments. Optical microscopy was also used to visualize precipitated magnetosomes within MDA-MB-231 cells. For that, the cells were incubated in the presence (or not) of suspensions containing either CM or IM. The cells were stained with Prussian blue, which precipitates in the presence of iron, producing a blue color in the micrographs, which reveals the presence of iron.

3. Results and discussion

3.1. The different types of bacterial magnetosomes chosen for magnetic hyperthermia treatment of tumors

In whole magnetotactic bacteria, the chains of magnetosomes only occupy a small portion of the total volume of a bacterium (~0.02%; Alphandéry et al., 2011d). A TEM image of a typical AMB-1 magnetotactic bacterium is shown in Fig. 1(a). Several chains of magnetosomes separated by more than ~100 nm are contained within this bacterium. Large regions of the bacterium are not occupied by chains of magnetosomes. Because of the low density of the chains of magnetosomes within whole magnetotactic bacteria, suspensions containing whole magnetotactic bacteria are expected to yield a low in vivo heating efficiency. In addition, the administration of whole inactive magnetotactic bacteria in humans is not recommended due to the presence of potentially toxic biologic materials such as bacterial DNA or endototoxins (Yoshino et al., 2008). For these two reasons, whole inactive magnetotactic bacteria were not tested in this study. In order to minimize the risks of toxicity and to enhance the heating efficiency, the bacterial magnetosomes were isolated from the bacteria.

The first type of bacterial magnetosomes tested for magnetic hyperthermia consisted of chains of magnetosomes extracted from AMB-1 magnetotactic bacteria, CM. Fig. 1(b) shows a TEM image of a suspension of CM deposited on top of a carbon grid. The extraction of the chains of magnetosomes from the bacteria yields an increase in the concentration of the chains of magnetosomes (Fig. 1(a) and (b)). The magnetosome chains also appear to be longer than in whole bacteria. When chains of magnetosomes are extracted from the magnetotactic bacteria, they interact with each other in such a way that they form longer chains. This type of interaction yields a homogeneous distribution of CM within the substrate (Fig. 1(b)). To assess the stability of CM mixed in water, their zeta potential was measured as a function of pH by dynamic laser light scattering (DLS) on a Nano-ZS (Red Badge) ZEN 3600 device (Malvern Instruments, Malvern, UK). For a suspension of CM, which is homogenized by sonication, Fig. 2(a) shows that the variations of the zeta potential as a function of pH is very similar to that obtained for a non sonicated suspension of CM. This indicates the good stability of the suspension of CM mixed in water. To examine if CM have kept the biological material surrounding them after extraction, infra-red absorption measurements were carried out on CM. Fig. 2(b) depicts the infra-red absorption spectrum of a powder containing a lyophilized suspension of chains of magnetosomes solubilized with KBr. It shows two absorption peaks at 1650 cm^{-1} (peak 1, Fig. 2(b)) and 1530 cm^{-1} (peak 2, Fig. 2(b)), which arise from the Amide I and Amide II bands and are due to the absorption of proteins (Diem et al., 1999; Han et al., 2008; Song et al., 2008). The peaks at 1250 cm^{-1} (peak 3, Fig. 2(b)) and 1050 cm^{-1} (peak 4, Fig. 2(b)) can either be attributed to the absorption of lipopolysaccharide (LPS) or phospholipids (Song et al., 2008; Abramson et al., 1965), both located within the magnetosome membrane (Yoshino et al., 2008). The peak at 580 cm^{-1} (peak 5, Fig. 2(b)) is attributed to maghemite (Predoi et al., 2010). These results suggest that both the filament binding the magnetosomes together, which is made of proteins such as MamJ or MamK (Draper et al., 2011; Scheffel et al., 2006), and the bilayer surrounding the individual magnetosomes, which is composed of LPS and phospholipids (Xie et al., 2009), are

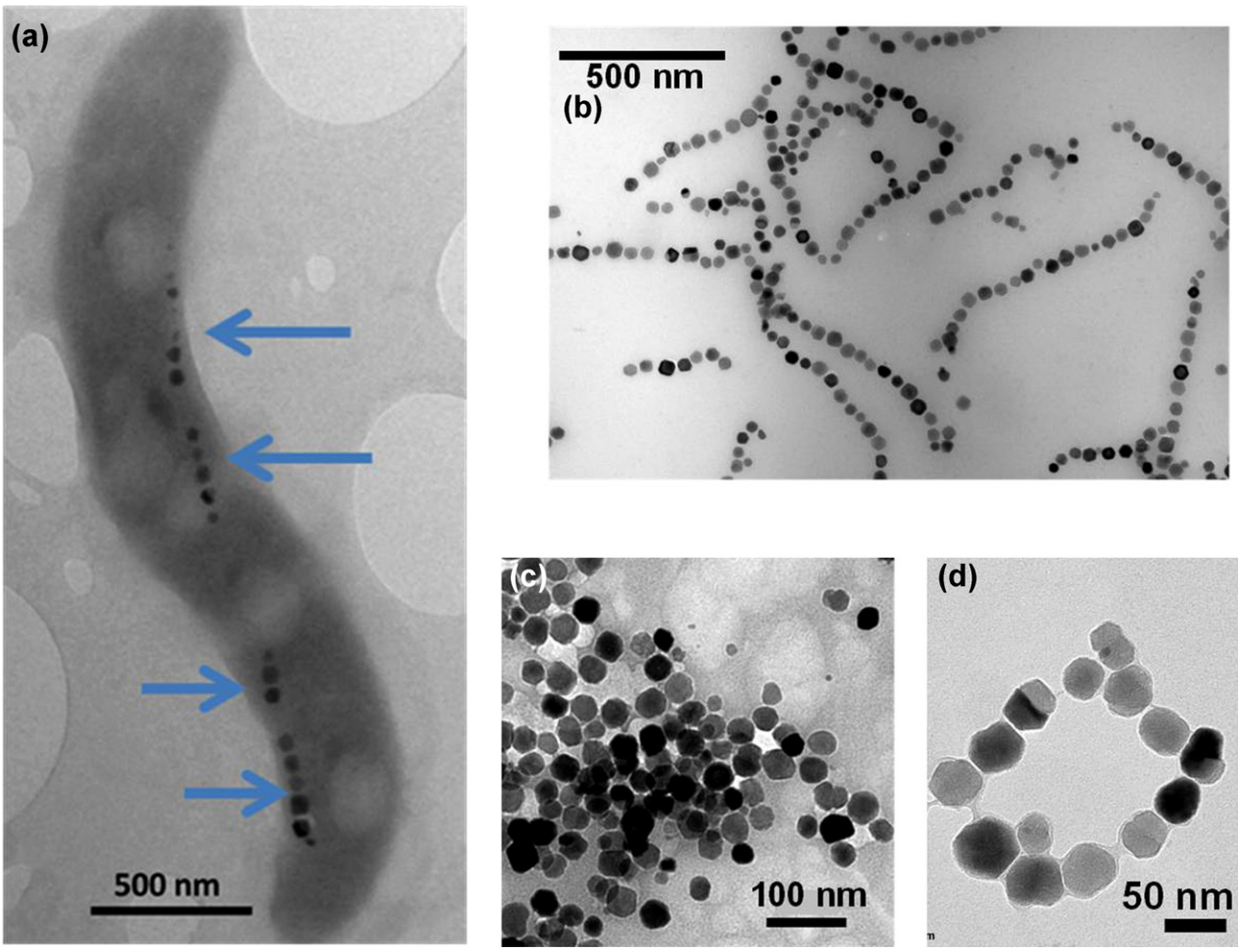

Fig. 1. (a) Transmission electron microscopy image of a typical whole inactive magnetotactic bacterium deposited on top of a carbon grid. The magnetosomes are designated by blue arrows. (b) Transmission electron microscopy image of suspensions of chains of magnetosomes, isolated from magnetotactic bacteria, and deposited on top of a carbon coated copper grid. (c) Transmission electron microscopy images of individual magnetosomes detached from the chains by heat and SDS treatment showing a typical aggregate. (d) Transmission electron microscopy images of individual magnetosomes detached from the chains by heat and SDS treatment showing a loop. (For interpretation of the references to color in this figure legend, the reader is referred to the web version of the article.)

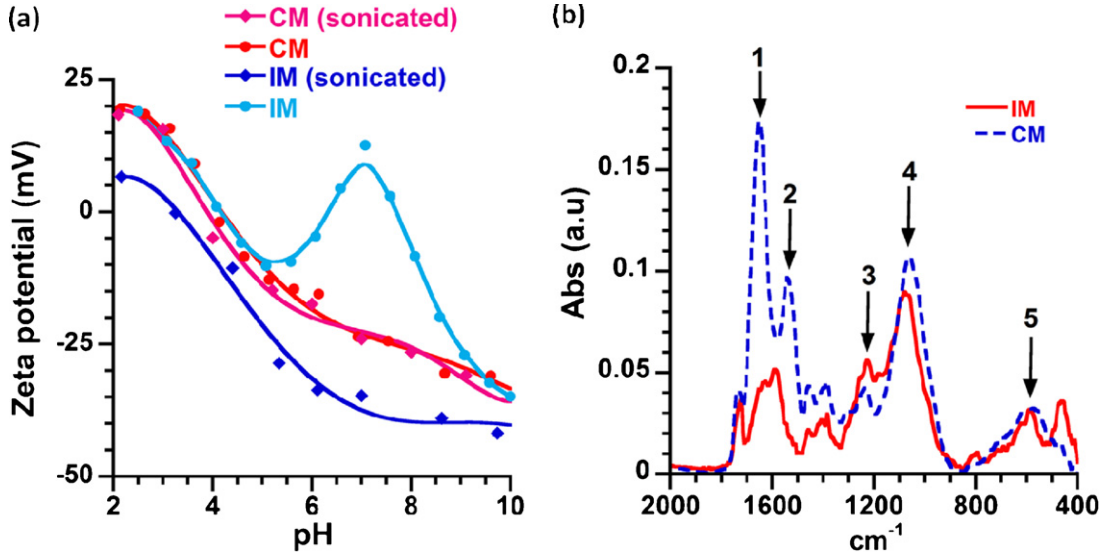

Fig. 2. (a) Zeta potential of suspensions of chains of magnetosomes and individual magnetosomes as a function of pH. The measurements were carried out with suspensions containing bacterial magnetosomes either mixed homogenously by sonication, designated by (sonicated), or not mixed. (b) Infrared absorption spectra of powders containing lyophilized suspensions of CM or IM embedded within a KBr matrix.

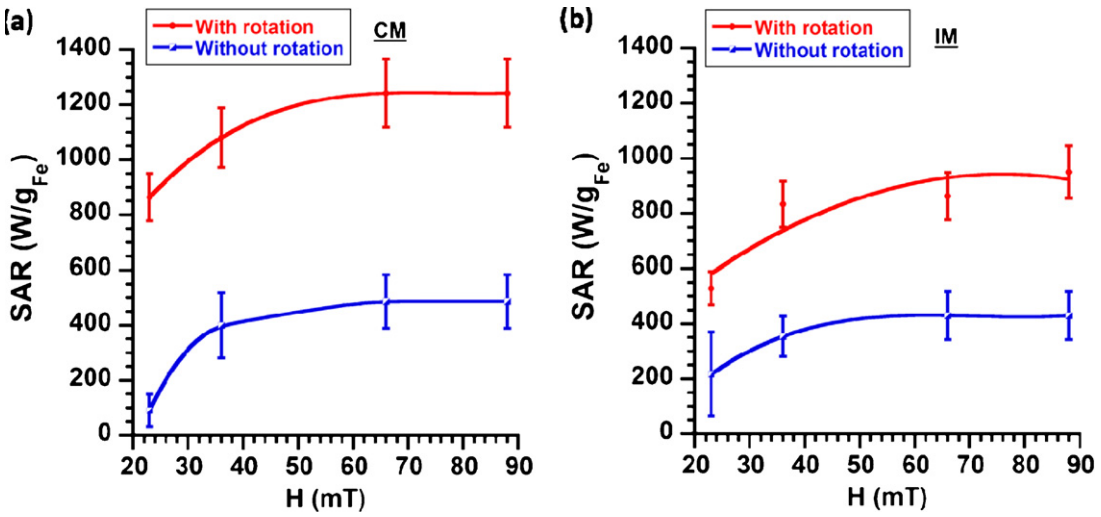

Fig. 3. (a) Specific absorption rate (SAR) of suspensions of chains of magnetosomes, which are able (or not if embedded in a gel or deposited on a solid substrate) to rotate under the application of an alternating magnetic field. (b) SAR of suspensions of individual magnetosomes, which are able (or not) to rotate under the application of an alternating magnetic field.

contained within CM. After extraction, the magnetosome chains have kept the lipid bi-layer surrounding each magnetosome and the filament binding the magnetosomes together.

To obtain suspensions of magnetosomes, which are similar to the chemically synthesized iron oxide nanoparticles, i.e. not arranged in chains, IM have been prepared by heating a suspension of CM at 90 °C during 5 h in the presence of 1% SDS. TEM images of a suspension of IM deposited on top of a carbon grid are presented in Fig. 1(c) and (d). It shows either assemblies of magnetosomes, which are much more aggregated than the chains of magnetosomes (Fig. 1(c)), or loops (Fig. 1(d)). At pH = 7, Fig. 2(a) shows that suspensions of IM possess very different values of their zeta potential depending on whether or not they are mixed homogeneously by sonication. When IM are mixed homogenously in solution, they possess a negative zeta potential of ∼−35 mV at pH ∼ 7 (Sunderland et al., 2006). When they are not sonicated, the IM zeta potential is 10 mV at pH ∼ 7. The different values of the zeta potential suggest that IM easily form aggregates in solution and are therefore unstable in the absence of sonication (Sunderland et al., 2006). The infra-red absorption spectrum of a powder containing a lyophilized suspension of IM integrated in a KBr matrix is presented in Fig. 2(b). It shows Amide I and Amide II peaks (peaks 1 and 2, Fig. 2(b)), suggesting that most of the proteins contained in the filament binding the magnetosomes together have been removed. The relatively strong peaks at 1050 cm^{-1} and 1240 cm^{-1} suggest that the bi-layer surrounding each magnetosome has not been significantly removed during the heat treatment in the presence of a detergent.

3.2. SAR of the different suspensions of bacterial magnetosomes

The SAR of suspensions containing IM and CM was measured in two situations in which the bacterial magnetosomes were either able or unable to rotate under the application of an AMF (Alphandéry et al., 2011a). For the bacterial magnetosomes mixed in water and able to rotate, Fig. 3(a) and (b) shows that the amount of heat produced by the CM is larger than that produced by the IM. This behavior could be explained by the fact that CM are less prone to aggregation and therefore rotate more easily than IM under the application of an AMF. This analysis is further supported by the TEM image presented in Fig. 1(b), which clearly shows that CM do not aggregate by contrast to IM (Fig. 1(c)). For the bacterial magnetosomes mixed in water, the higher value of the SAR obtained for CM compared with IM could therefore be explained by a contribution of the rotation to the heat production, which is more significant for CM than for IM. By contrast, when CM and IM are fixed (either in a gel or on a solid substrate (Alphandéry et al., 2011a)), unable to rotate, mixed homogenously and exposed to the same AMF as above, IM produce a relatively similar amount of heat than CM (Fig. 3(b)) (Alphandéry et al., 2011a). These results suggest that when the rotation of the magnetosomes is not taking part in the mechanism of heat production, which is most probably the case in vivo, the quantity of heat generated by CM or IM is not only due to the magnetosome SAR but also to the spatial distribution of the magnetosomes.

3.3. Percentage of inhibition of HeLa and MDA-MB-231 cells incubated in the presence of CM or IM

To compare the anti-tumoral activity of CM with that of IM, CM and IM were incubated in the presence of HeLa and MDA-MB-231 cells. The percentage of inhibition of cellular proliferation was then measured in the presence (or not) of an AMF. The results are presented for two suspensions of bacterial magnetosomes (CM or IM) with a concentration fixed at 0.125 mg/mL. In the absence of application of an AMF, the percentages of inhibition of MDA-MB-231 and HeLa cells incubated in the presence of CM or IM were as low as 2% and 10% (Fig. 4(a)), respectively. When these cancer cells were incubated in the presence of the CM and exposed to an AMF of frequency 198 kHz and average magnetic field strength of 20 mT and 30 mT, the percentages of inhibition increased by factors of ∼3 to ∼5 for the HeLa cells and ∼7 to ∼16 for the MDA-MB-231 cells (Fig. 4(a)). By contrast, when these cancer cells were incubated in the presence of IM and exposed to the same AMF as above, the percentage of inhibition of these cells remained almost identical (Fig. 4(a)). A similar type of behavior was observed when MDA-MB6231 and HeLa cells were incubated in the presence of CM and IM at higher iron oxide concentrations of 1 mg/mL (Suppl. Fig. 1(a)) and 0.5 mg/mL (Suppl. Fig. 1(b)). These results indicate that under the application of an AMF, CM yield a higher percentage of cell inhibition than IM.

3.4. Penetration of the chains of magnetosomes within the cancer cells under the application (or not) of an alternating magnetic field

We examine if the different efficiencies observed between CM and IM are due to a different faculty of penetration within the cancer cells of these two types of bacterial magnetosomes. We first

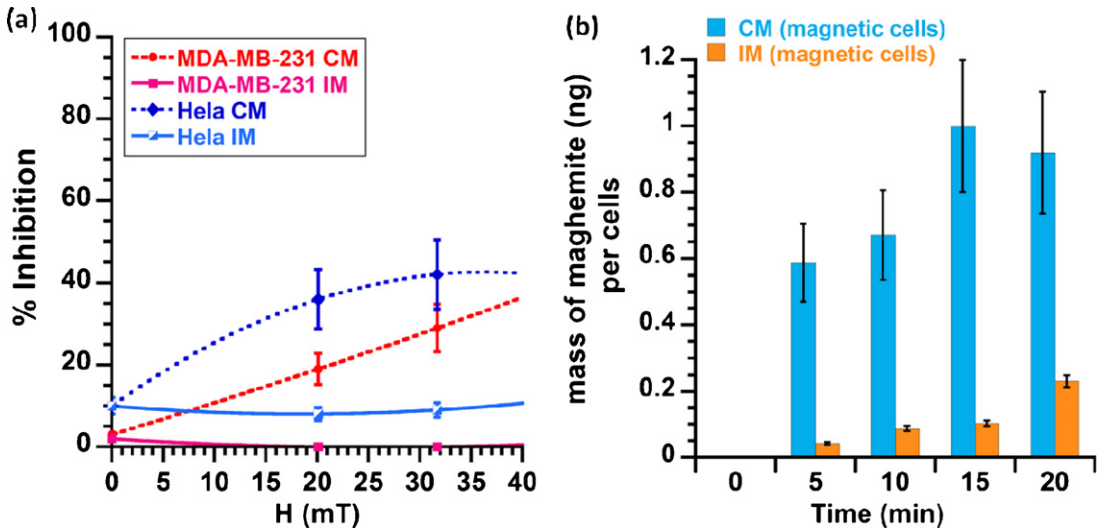

Fig. 4. (a) Percentage of inhibition of HeLa and MDA-MB-231 cells incubated in the presence of CM and IM as a function of the magnetic field strength. (b) Mass of maghemite internalized within MDA-MB-231 cells incubated in the presence of IM and CM and exposed to an alternating magnetic field of frequency 198 kHz and average field strength of 20 mT during 5–20 min.

study if the application of an AMF induces the internalization of CM or IM within the cancer cells. To be able to estimate the magnetization of MDA-MB-231 cells, the latter had to be kept free and not fixed. The cells were incubated in the presence of the CM and IM and exposed to the same AMF as above. The cancer cells were then washed with water to remove CM and IM located at their surface and the percentage of magnetic cells was then measured. Following application of an AMF of frequency 198 kHz during 5–20 min, Fig. 4(b) shows that the mass of maghemite per magnetic cell is always much higher for the cells incubated in the presence of CM than for those incubated in the presence of IM. This result suggests that under the application of an AMF, CM penetrate much more within the cancer cells than IM. Moreover, the high cellular magnetization, which can be reached in the presence of CM under the application of an AMF, could explain the high efficiency of CM for magnetic hyperthermia treatment of tumors.

We also study the internalization of CM and IM within the cancer cells as a function of the incubation time in the absence of an AMF. For that, the cells had to be fixed on top of a solid substrate. For a very short incubation time of less than 30 s, Fig. 4(b) shows that neither CM nor IM penetrate within MDA-MB-231 cells. Suspensions containing CM and IM were then incubated in the presence of MDA-MB-231 cells for a longer incubation time of 24 h. The cells were deposited on top of a carbon grid substrate and imaged under

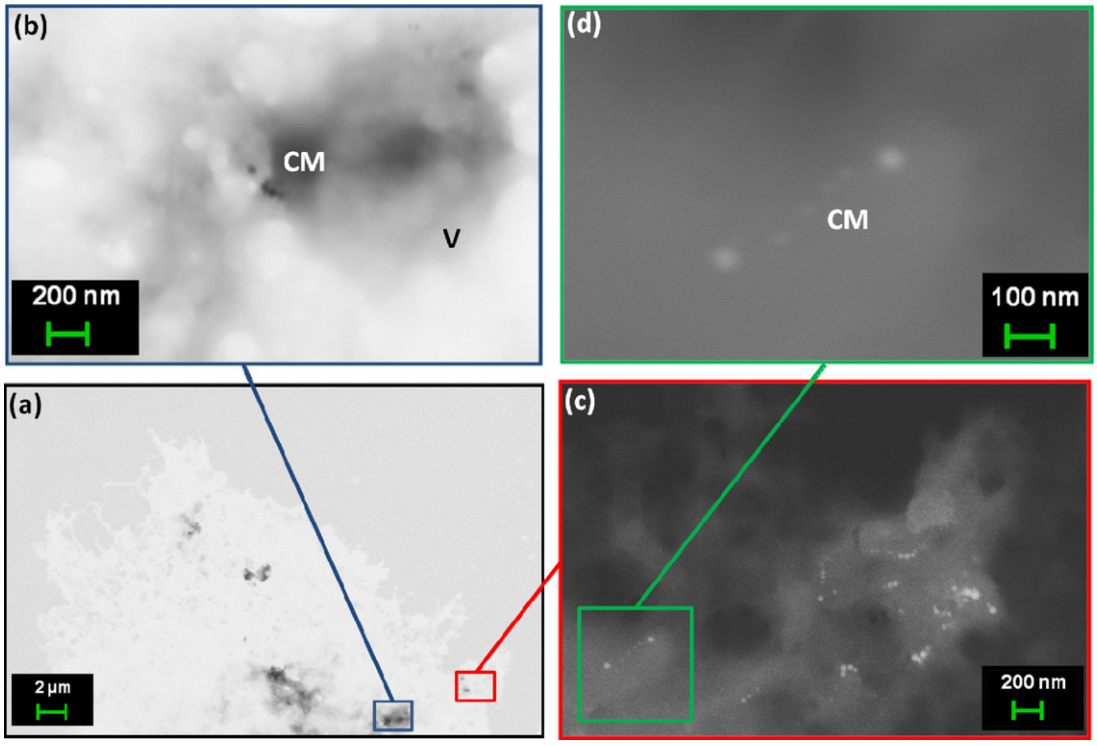

Fig. 5. Scanning electron microscopy image of a MDA-MB-231 cell incubated in the presence of CM. V designates a vesicle.

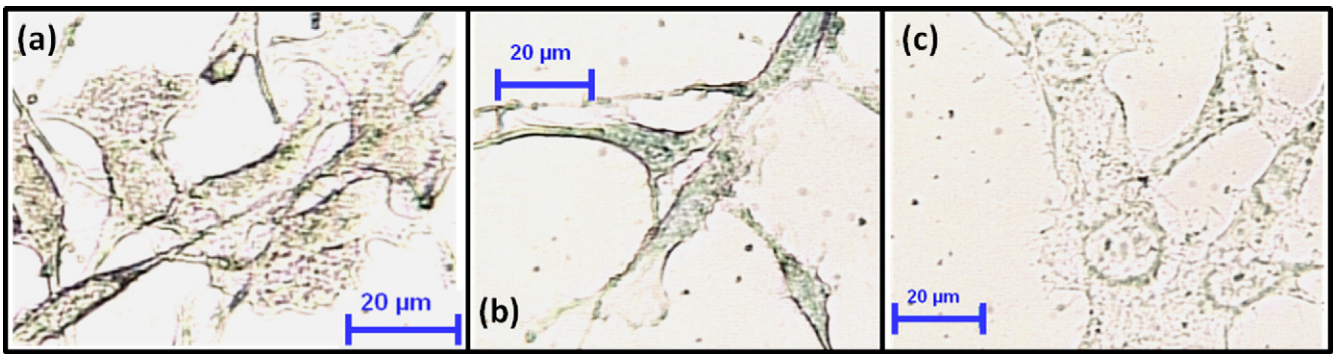

Fig. 6. Confocal optical microscopic images of cancer cells stained with Prussian blue and incubated in the absence of magnetosomes (a), in the presence of CM (b), and in the presence of IM (c).

scanning electron microscopy. Fig. 5(a) shows a portion of a typical MDA-MB-231 cell. Enlargements of two regions of the cell in which CM are observed are presented in Fig. 5(b) and (c). Since CM are observed within intracellular vesicles, designated as V in Fig. 5(b), which can be lysosomes or endosomes, CM are internalized within the cancer cell. The chain of magnetosome surrounded by a green box in Fig. 5(c) and (d) contains two large magnetosomes at its end and several small magnetosomes at the middle. This type of magnetosome arrangement is clearly different from that observed for the magnetosome chains, which are not incubated in the presence of cancer cells (Fig. 1(b)). It could be due to the degradation of the chains of magnetosomes by the cells following their internalization. Another reason why CM are internalized within the cells and not bound at the cell surface comes from the fact that the cells were washed prior to the observation by scanning electron microscopy. The presence of CM within the cells was further confirmed by EDX measurements, which revealed the presence of iron oxide in the region where CM were detected (Suppl. Fig. 3). By contrast to the behavior observed with CM, IM were not observed within the MDA-MB-231 cell (Suppl. Fig. 2). The EDX measurements confirmed this behavior (Suppl. Fig. 3). They showed that iron was not detected in the cellular regions with presumably no magnetosomes.

The internalization of CM within the cancer cells for a sufficiently long incubation time of 24 h was further confirmed by optical microscopy. Fig. 6 shows optical microscopy observations of MDA-MB-231 cells incubated in the absence of magnetosomes (Fig. 6(a)), in the presence of CM during 24 h (Fig. 6(b)) or in the presence of IM during 24 h (Fig. 6(c)). For MDA-MB-231 cells incubated in the absence of magnetosomes or in the presence of IM, no Prussian blue coloration was observed within the cells. By contrast, for the MDA-MB-231 cells incubated in the presence of the CM, Prussian blue coloration was observed within the cells. These results agree with those presented above (Fig. 5) and suggest that CM penetrate within the cells by contrast to IM, which remain located outside of the cells.

3.5. *Explanation for the high efficiency of the chains of magnetosomes*

Altogether, these results indicate that CM penetrate more easily within the cancer cells than IM. While the internalization within the cancer cells did not occur with IM, it was observed for CM in two conditions, either when an AMF of 198 kHz and average field strength of 20 mT was applied during 5–20 min and/or when the cells were incubated with CM for a sufficiently long time of 24 h. The internalization of CM within the cancer cells could occur by a mechanism of endocytosis or by effective diffusion through the cell membrane. The mechanism of effective diffusion through the cell membrane could be favored by a temperature increase taking place during the application of the AMF, which would

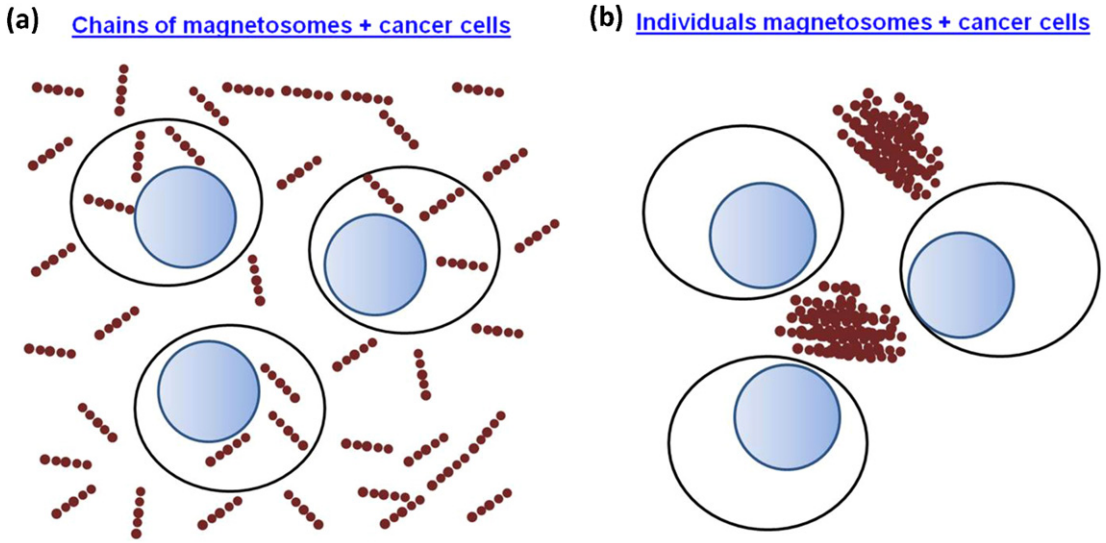

Fig. 7. Conceptual summary describing the effect of aggregation on the magnetosome spatial distribution and on the magnetosome penetration within cancer cells. The magnetosomes are either CM (a) or IM (b).

make the cell membrane permeable. This result agrees with previous studies, which showed that negatively charged maghemite nanoparticles penetrate within cancer cells (Wilhelm et al., 2003). Since intra-cellular heating presumably efficiently damages cellular components, it may be a more efficient mechanism of cell destruction than extra-cellular heating. The higher efficiency of CM compared with that of IM could therefore be explained by the fact that CM internalize within the cancer cells by contrast to IM, which mostly remain located outside of the cells (Villanueva et al., 2009). Poorly efficient internalization of IM may be related to the more aggregated state of IM compared with that of CM as was observed in two cases, i.e. when suspensions of CM and IM were deposited on top of a carbon grid (Fig. 1(b) and (c)) and in vivo when suspensions of CM and IM were administered within tumors xeno-grafted under the skin of mice and heated under the application of an AMF (Alphandéry et al., 2011c). A schematic summary showing the different distributions of CM and IM in the presence of cancer cells is proposed in Fig. 7(a) and (b). The better internalization and more homogenous distribution of CM than IM could provide a reasonable explanation for the higher anti-tumoral efficiency observed for CM than for IM (Alphandéry et al., 2011c).

4. Conclusion

In conclusion, we have studied two types of bacterial magnetosomes extracted from AMB-1 magnetotactic bacteria, the magnetosomes organized in chains and those forming individual magnetosomes detached from the chains by heat and chemical treatment. We have shown that chains of magnetosomes were more efficient than individual magnetosomes in inhibiting cancer cell proliferation under application of an alternating magnetic field. We have suggested that this increased efficiency was related to much less particle aggregation for the magnetosome chains than for the individual magnetosomes and as a consequence to a better faculty for the chains of magnetosomes than for the individual magnetosomes to internalize within the cancer cells. This paper clearly highlights the importance of nanoparticle distribution for efficient magnetic hyperthermia. It shows that the use of nanoparticles with high SAR is not sufficient to yield efficient magnetic hyperthermia.

Acknowledgments

François Guyot does not claim any inventive contribution in this work. We thank the company NOVAcyt for giving us the NOVAprep product free of charge.

Appendix A. Supplementary data

Supplementary data associated with this article can be found, in the online version, at http://dx.doi.org/10.1016/j.ijpharm.2012.06.015.

References

Abramson, M.B., Norton, W.T., Katzman, R., 1965. Study of ionic structures in phospholipids by infrared spectra. J. Biol. Chem. 240, 2389–2395.

Alphandéry, E., Ngo, A.T., Lefèvre, C., Lisiecki, I., Wu, L.F., Pileni, M.P., 2008. Difference between the magnetic properties of the magnetotactic bacteria and those of the extracted magnetosomes: influence of the distance between the chains of magnetosomes. J. Phys. Chem. C 112, 12304–12309.

Alphandéry, E., Faure, S., Chebbi, I., 2011a. Treatment of cancer or tumor induced by the release of heat generated by various chains of magnetosomes extracted from magnetotactic bacteria and submitted to an alternative magnetic field. Int. Patent No. 061259.

Alphandéry, E., Carvallo, C., Menguy, N., Chebbi, I., 2011b. Chains of cobalt doped magnetosomes extracted from AMB-1 magnetotactic bacteria for application in alternative magnetic field cancer therapy. J. Phys. Chem. C 115, 11920–11924.

Alphandéry, E., Faure, S., Seksek, O., Guyot, F., Chebbi, I., 2011c. Chains of magnetosomes extracted from AMB-1 magnetotactic bacteria for application in alternative magnetic field cancer therapy. ACS Nano 5, 6279–6296.

Alphandéry, E., Faure, S., Raison, L., Duguet, E., Howse, P.A., Bazylinski, D.A., 2011d. Heat production by bacterial magnetosomes exposed to an oscillating magnetic field. J. Phys. Chem. C 115, 18–22.

Bordelan, D.E., Cornefo, C., Grüttner, C., Wesphal, F., Deweese, T.L., Ivkov, R., 2011. Magnetic nanoparticle heating efficiency reveals magneto-structural differences when characterized with wide ranging and high amplitude alternative magnetic fields. J. Appl. Phys. 109, 124904.

DeNardo, S.J., DeNardo, G.L., Natarajan, A., Miers, L.A., Foreman, A.R., Gruettner, C., Adamson, G.N., Ivkov, R., 2007. Thermal dosimetry predictive of efficacy of ^{111}In-ChL6 nanoparticle AMF-induced thermoablative therapy for human breast cancer in mice. J. Nucl. Med. 48, 437–444.

Diem, M., Bodydston-White, S., Chiriboga, L., 1999. Infrared spectroscopy of cells and tissues: shining light onto a novel subject. Appl. Spectrosc. 53, 148A–161A.

Draper, O., Byrne, M.E., Li, Z., Keyhani, S., Barrozo, J.C., Jensen, G., Komeili, A., 2011. MamK, a bacterial actin, forms dynamic filament in vivo that are regulated by the acidic proteins MamJ and LimJ. Mol. Microbiol. 82, 342–354.

Han, L., Li, S.Y., Yang, Y., Zhao, F.M., Huang, J., Chang, J., 2008. Research on the structure and performance of bacterial magnetic nanoparticles. J. Biomater. Appl. 22, 433–448.

Hergt, R., Dutz, S., 2007. Magnetic particle hyperthermia—biophysical limitations of a visionary tumour therapy. J. Magn. Magn. Mater. 311, 187–192.

Hergt, R., Hiergeist, R., Zeisberger, M., Schüler, D., Heyen, U., Hilger, I., Kaiser, W.A., 2005. Magnetic properties of bacterial magnetosomes as potential diagnostic and therapeutic tools. J. Magn. Magn. Mater. 293, 80–86.

Hergt, R., Dutz, S., Müller, R., Zeisberger, M., 2006. Magnetic hyperthermia: nanoparticle magnetism and material development for cancer therapy. J. Phys.: Condens. Matter 18, S2919–S2934.

Hergt, R., Dutz, S., Röder, M., 2008. Effects of size distribution on hysteresis losses of magnetic nanoparticles for hyperthermia. J. Phys.: Condens. Matter 20, 385214.

Ivkov, R., DeNardo, S.J., Daum, W., Foreman, A.R., Goldstein, R.C., Nemkov, V.S., DeNardo, V., 2005. Application of high amplitude alternating magnetic fields for heat induction of nanoparticles localized in cancer. Clin. Cancer Res. 11, 7093–7103.

Johannsen, M., Gnevekow, U., Eckelt, L., Feussner, A., Waldöfner, N., Scholz, R., Deger, S., Wust, P., Loening, S.A., Jordan, A., 2005. Clinical hyperthermia od prostate cancer using magnetic nanoparticles: presentation of a new interstitial technique. Int. J. Hyperthermia 21, 637–647.

Johannsen, M., Gnevekow, U., Thiesen, B., Taymoorian, K., Cho, C.H., Waldöfner, N., Scholz, R., Jordan, A., Loening, S.A., Wust, P., 2007. Thermotherapy of prostate cancer using magnetic nanoparticles: feasibility, imaging, and three-dimensional temperature distribution. Eur. Urol. 52, 1653–1662.

Kawai, N., Ito, A., Nakahara, Y., Futakuchi, M., Shirai, T., Honda, H., Kobayasi, T., Kohri, K., 2005. Anticancer effect of hyperthermia on prostate cancer mediated by mediated by magnetite cationic liposomes and immune-response induction in transplanted syngeneic rats. The Prostate 64, 373–381.

Kawai, N., Futakuchi, M., Yoshida, T., Ito, A., Sato, S., Naiki, T., Honda, H., Shirai, T., Kohri, K., 2008. Effect of heat therapy using magnetic nanoparticles conjugated with cationic liposomes on prostate tumor in bone. The Prostate 68, 784–792.

Kikumori, T., Kobayashi, T., Sawaki, M., Imai, T., 2009. Anti-cancer effect of hyperthermia on breast cancer by magnetite nanoparticle-loaded anti-HER2 immunoliposomes. Breast Cancer Res. Treat. 113, 435–441.

Maier-Hauff, K., Ulrich, F., Nestler, D., Niehoff, H., Wust, P., Thiesen, B., Orawa, H., Brudach, V., Jordan, A., 2011. Efficacy and safety of intratumoral thermotherapy using magnetic iron-oxide nanoparticles combined with external beam radiotherapy on patients with recurrent glioblastoma multiforme. J. Neurooncol. 103, 317–324.

Mosmann, T., 1938. Rapid colorimetric assay for cellular growth and survival: application to proliferation and cytotoxicity assays. J. Immunol. Methods 65, 55–63.

Predoi, D., Andronescu, E., Radu, M., Munteanu, M.C., Dinischiotu, A., 2010. Synthesis and characterization of bio-compatible maghemite nanoparticles. Digest J. Nanomater. Biostruct. 5, 779–786.

Scheffel, A., Gruska, M., Faivre, D., Linaroudis, A., Plitzko, J., Schüler, D., 2006. An acidic protein aligns magnetosomes along a filamentous structure in magnetotactic bacteria. Nature 440, 110–114.

Song, H.P., Li, X.G., Sun, J.S., Xu, S.M., Han, X., 2008. Application of a magnetotactic bacterium, *Stenotrophomas* sp. to the removal of Au(III) from contaminated wastewater with a magnetic separator. Chemosphere 72, 616–621.

Sunderland, C.J., Steiert, M., Talmadge, J.E., Derfus, A.M., Barry, S.E., 2006. Targeted nanoparticles for detecting and treating cancer. Drug Dev. Res. 67, 70–93.

Timko, M., Dzarova, A., Kovac, J., Skumiel, A., Józefcak, A., Hornowski, T., Gojżewski, H., Zavisova, V., Koneracka, M., Sprincova, A., Strbak, O., Kopcansky, P., Tomasovicova, N., 2009. Magnetic properties and heating effect in bacterial magnetic nanoparticles. J. Magn. Magn. Mater. 321, 1521–1524.

Villanueva, A., Canete, M., Roca, A.G., Calero, M., Veintemillas-Verdaguer, S., Serna, C.J., Del Puerto Morales, M., Miranda, R., 2009. The influence of surface functionalization on the enhanced internalization of magnetic nanoparticles in cancer cells. Nanotechnology 20, 115103.

Wilhelm, C., Billotey, C., Roger, J., Pons, J.N., Bacri, J.C., Gazeau, F., 2003. Intracellular uptake of anionic superparamagnetic nanoparticles as a function of their surface coating. Biomaterials 24, 1001–1011.
Wolfe, R.S., Thauer, R.K., Pfennig, N.A., 1987. A "capillary racetrack" method for isolation of magnetotactic bacteria. FEMS Microbiol. Ecol. 45, 31–35.
Xie, J., Chen, K., Chen, X., 2009. Production, modification and bio-applications of magnetic nanoparticles gestates by magnetotactic bacteria. Nano Res. 2, 261–278.
Yoshino, T., Hirabe, H., Takahashi, M., Kuhara, M., Takeyama, H., Matsunaga, T., 2008. Magnetic cell separation using nano-sized bacterial magnetic particles with reconstructed magnetosome membrane. Biotechnol. Bioeng. 101, 470–477.
Zhao, Q., Wang, L., Cheng, R., Mao, L., Arnold, R.D., Howerth, E.W., Chen, Z.G., Platt, S., 2012. Magnetic nanoparticle-based hyperthermia for head and neck cancer in mouse models. Theranostics 2, 113–121.